Biomaterials-aided mandibular reconstruction using in vivo bioreactors

Alexander M. Tatara[a,b], Gerry L. Koons[a,b], Emma Watson[a,b], Trenton C. Piepergerdes[a], Sarita R. Shah[a,b], Brandon T. Smith[a,b], Jonathan Shum[c], James C. Melville[c], Issa A. Hanna[c], Nagi Demian[c], Tang Ho[d], Anthony Ratcliffe[e], Jeroen J. J. P. van den Beucken[f], John A. Jansen[f], Mark E. Wong[c], and Antonios G. Mikos[a,1]

[a]Department of Bioengineering, Rice University, Houston, TX 77030; [b]Medical Scientist Training Program, Baylor College of Medicine, Houston, TX 77030; [c]Department of Oral and Maxillofacial Surgery, The University of Texas Health Science Center at Houston, Houston, TX 77030; [d]Department of Otorhinolaryngology, The University of Texas Health Science Center at Houston, Houston, TX 77030; [e]Synthasome, Inc., San Diego, CA 92019; and [f]Department of Biomaterials, Radboud University Medical Center, 6525 EX Nijmegen, The Netherlands

Edited by Kristi S. Anseth, University of Colorado Boulder, Boulder, CO, and approved February 15, 2019 (received for review November 10, 2018)

Large mandibular defects are clinically challenging to reconstruct due to the complex anatomy of the jaw and the limited availability of appropriate tissue for repair. We envision leveraging current advances in fabrication and biomaterials to create implantable devices that generate bone within the patients themselves suitable for their own specific anatomical pathology. The in vivo bioreactor strategy facilitates the generation of large autologous vascularized bony tissue of customized geometry without the addition of exogenous growth factors or cells. To translate this technology, we investigated its success in reconstructing a mandibular defect of physiologically relevant size in sheep. We fabricated and implanted 3D-printed in vivo bioreactors against rib periosteum and utilized biomaterial-based space maintenance to preserve the native anatomical mandibular structure in the defect site before reconstruction. Nine weeks after bioreactor implantation, the ovine mandibles were repaired with the autologous bony tissue generated from the in vivo bioreactors. We evaluated tissues generated in bioreactors by radiographic, histological, mechanical, and biomolecular assays and repaired mandibles by radiographic and histological assays. Biomaterial-aided mandibular reconstruction was successful in a large superior marginal defect in five of six (83%) sheep. Given that these studies utilized clinically available biomaterials, such as bone cement and ceramic particles, this strategy is designed for rapid human translation to improve outcomes in patients with large mandibular defects.

bone | tissue engineering | craniofacial | bioreactor | in vivo

From a functional, psychological, and socioeconomic standpoint, large mandibular defects have devastating effects on quality of life. Restoring both mandibular function and aesthetic structure is key to a successful outcome. The current gold standard for mandibular reconstruction is the fibular flap, in which a segment of the fibula is harvested, manually shaped to the size and geometry of the mandibular defect in the operating room, and transferred as a bony free flap to the mandible (1, 2). This approach is limited by the volume and geometry of the donor tissue. In addition, patients may experience donor site morbidity at the site of the harvested tissue (3). Therefore, there is a clinical need for new strategies to facilitate mandibular reconstruction.

To that effect, we and others have investigated in vivo bioreactors for the generation of engineered autologous vascularized bony free flaps (4–7). These bioreactors are implanted at a site ectopic to the defect, such as against the periosteum of the rib cage. By filling the bioreactors with an osteoconductive biomaterial, native cell populations can be stimulated to migrate into the bioreactors and generate bony tissue. This strategy utilizes acellular scaffolds without the need for exogenous cells or supplemented growth factors. As the tissues grow to fill the size and shape of the bioreactor (5, 6), customized vascularized flaps can be designed for specific geometries on a patient-to-patient basis.

In current clinical practice, definitive mandibular resection can be performed in two stages to treat underlying infection of the wound, to prepare suitable free flaps, or to stimulate a regenerative environment for the definitive reconstruction by promoting healthy soft tissue development over the defect site (8–10). To this effect, space maintainers have been successfully used to aid two-stage mandibular repair in human cases (10–12). Space maintainers are formulated from poly(methylmethacrylate) (PMMA), a currently regulated clinical biomaterial used as bone cement. In addition to preserving native facial contours and architecture by preventing scar tissue ingrowth into the defect, PMMA-based space maintainers induce the growth of an osteogenic membrane ("Masquelet technique") that aids in definitive reconstruction (13, 14). Furthermore, PMMA-based space maintainers can be fabricated to have porous architecture for the reconstruction of large mandibular defects. These porous bone space maintainers (PBSMs) promote healthy soft tissue growth in preclinical models and were used successfully in human cases (12, 15, 16). In addition, PBSMs have been engineered to locally release antibiotics into the defect site in a controlled and extended manner to prevent and/or treat infection (17), a common complication of mandibular injury due to the adjacent oral microbiome. Space maintainers are intended for temporary use

Significance

People may suffer large losses of mandibular (jaw) bone due to cancer, infection, trauma, congenital disease, or other disorders. The resulting bony defects are both aesthetically disfiguring and functionally disabling. We have designed a strategy to use biomaterials and 3D printing to leverage the body's own innate healing capacity to generate customized engineered tissues that fit the patient's defect. Using a large animal (sheep) model, we 3D printed bioreactors, filled them with biomaterial scaffold materials, and implanted them against the ribs to grow customized bony tissues. These tissues were then successfully surgically transplanted to repair a large defect in the sheep mandible. This approach results in tissue flaps with custom geometry and reduced risk of rejection.

Author contributions: A.M.T., G.L.K., E.W., T.C.P., S.R.S., B.T.S., J.S., J.C.M., I.A.H., N.D., T.H., J.J.J.P.v.d.B., J.A.J., M.E.W., and A.G.M. designed research; A.M.T., G.L.K., E.W., T.C.P., S.R.S., B.T.S., J.S., J.C.M., I.A.H., N.D., T.H., A.R., J.J.J.P.v.d.B., J.A.J., M.E.W., and A.G.M. performed research; A.M.T., G.L.K., E.W., T.C.P., B.T.S., J.J.J.P.v.d.B., J.A.J., M.E.W., and A.G.M. analyzed data; and A.M.T., G.L.K., E.W., T.C.P., and A.G.M. wrote the paper.

The authors declare no conflict of interest.

This article is a PNAS Direct Submission.

[1]To whom correspondence should be addressed. Email: mikos@rice.edu.

This article contains supporting information online at www.pnas.org/lookup/suppl/doi:10.1073/pnas.1819246116/-/DCSupplemental.

Published online March 18, 2019.

within a bony defect and can be safely removed during definitive reconstruction (12).

Lastly, efforts have been made to implement new developments in fabrication techniques for use in craniofacial tissue engineering. Specifically, the advent of 3D printing has facilitated the creation of devices with a complex size and shape based on patient-specific anatomical pathology (18, 19). Using data obtained from radiographic scans of patients, 3D printing holds the promise of a "personalized medicine" approach to the generation of implantable devices for patients with irregularly shaped tissue defects. Unlike the approach of 3D printing of an acellular construct for direct implantation in a defect site, this envisioned strategy allows for reconstruction of the mandibular defect with prefabricated, autologous, vascularized tissue that was generated in the patient's own body. This mitigates risks associated with implantation of an acellular scaffold or graft in the mandible, including infection and tissue dehiscence (1, 2).

In sum, our vision for biomaterials-aided mandibular reconstruction is as follows:

i) A patient presents with a large mandibular defect due to pathological injury, such as trauma, tumor resection, or infection (20).
ii) A 3D scan of the defect region is taken by computed tomography or MRI.
iii) Using the data obtained from radiology, bioreactors are three-dimensionally printed with the precise volume and geometry of the defect (19).
iv) The bioreactors are then filled with a biomaterial and implanted against the periosteum of the patient's rib cage or ilium (4). During the same operation, a porous space maintainer is implanted into the defect space to stimulate healthy soft tissue healing and prime the wound site for reconstruction while maintaining the patient's native facial contours.
v) Following several months of tissue growth within the bioreactor and formation of a healthy tissue envelope around the bioreactor, the space maintainer is removed and the mandible is reconstructed with tissue generated within the in vivo bioreactor.
vi) After definitive reconstruction, the transferred tissue integrates with the surrounding native mandible for regeneration of the defect.

In this study, this approach was evaluated in a large animal model of disease as outlined in Fig. 1. Sheep were implanted with 3D-printed bioreactors filled with either autograft (AG) or synthetic graft (SG) as scaffold material. Simultaneously, a challenging superior marginal defect was created in the right hemimandible of the sheep and treated with a PBSM. After 9 wk of biomaterial implantation, the PBSM was removed and tissue generated in the bioreactors was transferred to the mandibular defect as an engineered bone free tissue flap. Twelve weeks later (21 wk after the first surgical stage), the animals were killed and the mandibles were harvested. Radiological, histological, mechanical, and biomolecular assays were used to analyze bioreactor-generated tissue as a function of initial scaffold material. Reconstructed hemimandibles were compared with native contralateral hemimandibles by radiographic and histological assays. Our hypotheses were that use of synthetic biomaterial would result in equivalent generation of mineralized tissue compared with autologous graft within the bioreactors, and that the combination of space maintenance and 3D-printed in vivo bioreactors would result in successful mandibular reconstruction.

Results

Bioreactor Surgical Outcomes. Bioreactors were filled with either morcellized rib AG or commercially available bioceramic SG (Fig. 2*A*), and four bioreactors per animal were implanted successfully against the periosteum of alternating ribs (Fig. 2*B*). All animals tolerated the implantation procedure well with no issues during recovery. Upon harvest at 9 wk, the majority of bioreactors had generated bony tissue matching the geometry of the bioreactor (Fig. 2*C*).

In sum, six sheep were implanted with four bioreactors each (24 bioreactors in total). Six bioreactors were intended to generate tissue for mandibular reconstruction and were chosen to be filled with AG as that is the current gold standard biomaterial (21). Of the remaining 18 bioreactors implanted for tissue intended for analysis, nine were AG and nine were SG. By the end of 9 wk of implantation, two bioreactors in a single animal (one AG and one SG) were lost due to infection (culture of recovered purulent material demonstrated nonhemolytic gram-positive cocci) and two bioreactors did not generate solid tissues (two AG); thus, six AG bioreactors and eight SG bioreactors

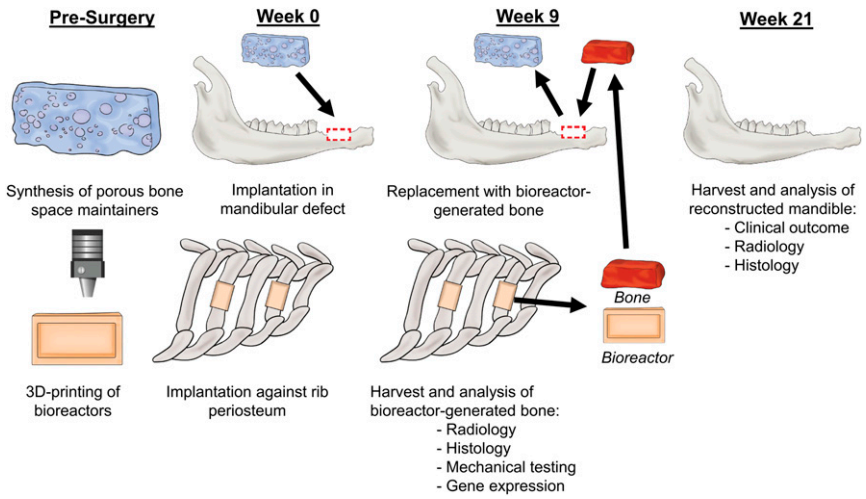

Fig. 1. Schematic of the use of the in vivo bioreactor strategy for reconstruction in a sheep model. PBSMs were fabricated, and bioreactors were 3D printed to the shape of the mandibular defect. At week 0, a defect was made in the mandible and four bioreactors were implanted against the periosteum of the rib. The mandibular defect space was preserved by insertion of the PBSM. At week 9, bioreactors were harvested for analysis or for use as vascularized free flaps in the reconstruction of the mandible. At week 21, the mandibles were harvested to analyze the success of the strategy for mandibular reconstruction.

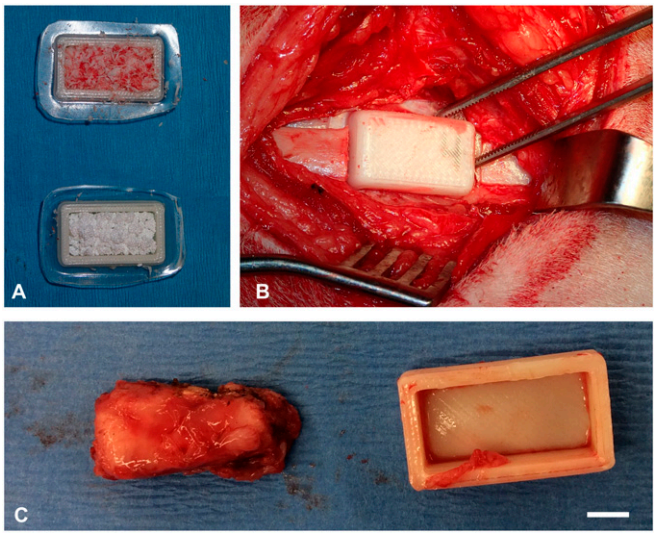

Fig. 2. Photographs of bioreactors. (*A*) 3D-printed bioreactors were filled with either autologous bone (*Top*) or SG (*Bottom*). (*B*) Filled bioreactors were implanted with their open face against the rib periosteum. (*C*) After 9 wk of implantation, tissue had grown within the implanted bioreactors and conformed to the dimensions of the 3D-printed bioreactor. (Scale bar: 5 mm.)

were available for subsequent analysis. Including the six AG bioreactors transferred to the mandibular defect, 20 of 24 (83.3%) of implanted bioreactors generated blocks of tissue with handling properties and mineralization sufficient for surgical reconstruction.

Mineralization of Tissues Generated in in Vivo Bioreactors. As shown in representative cross-sections of scaffold material before implantation (week 0) and postimplantation (week 9) (Fig. 3*A*), the amount and morphology of radiopaque material within the bioreactors evolved over the 9 wk of in vivo exposure. These differences were quantified with bone volume/total volume (BV/TV), trabecular thickness (Tb.Th.), trabecular number (Tb.N.), and trabecular spacing (Tb.Sp.) (Fig. 3 *B–E* and *SI Appendix*, Table S1).

Quantity and Quality of Bone Generated in in Vivo Bioreactors. Recovered bioreactor-generated tissues not used for mandibular reconstruction were processed for histology [AG ($n = 6$) and SG ($n = 8$); infected tissues were excluded]. Sections from bioreactor-generated tissues were analyzed by histological scoring and histomorphometry to determine the following: height of viable bone (fractional depth, a 2D measurement of the fraction of the bioreactor's height that was filled with viable bone tissue); relative surface area of remaining SG, bone, and total hard tissue; and histological scoring (*SI Appendix*, Table S2), including tissue type, tissue maturity, presence of osteoclasts within tissues, intactness of SG, and amount of scaffold that became encapsulated with new tissue (Fig. 4 and *SI Appendix*, Tables S3 and S4). As shown in Fig. 4 *A–D*, both AG and SG were capable of supporting new viable mineralized tissues. Of note, as described in previous work (5, 6), bioreactors initially filled with AG had nonzero measurements of remaining SG in Fig. 4*F* due to artifact (unbiased thresholding, including cellular debris, detected as remaining SG).

Mechanical Properties of Tissues Generated in in Vivo Bioreactors. Cube-shaped specimens were cut from bioreactor-generated tissues (infected tissues excluded) as well as native sheep rib and were subjected to compressive testing (Fig. 5): for compressive modulus [rib ($n = 6$), AG ($n = 6$), and SG ($n = 8$)] and for compressive strength [rib ($n = 6$), AG ($n = 4$), and SG ($n = 8$), as two AG specimens did not fracture or have stress/strain curves with deflection through the 2% offset yield line (*SI Appendix*, Fig. S1), and therefore did not have calculatable strength].

Rib, AG, and SG compressive strengths were 6.44 ± 4.31 MPa, 4.77 ± 2.75 MPa, and 2.06 ± 1.25 MPa, respectively. Rib, AG, and SG compressive moduli were 200.01 ± 157.65 MPa, 75.69 ± 47.60 MPa, and 58.02 ± 45.58 MPa, respectively. The compressive strength and modulus of bone from the rib were significantly greater than SG, but there were no other differences among groups.

Mandibular Defect Creation and PBSM Implantation Outcomes. A superior marginal defect was created in each sheep's diastema (Fig. 6*A*). The length of the defect was limited by each animal's unique anatomy and ranged from 15.0 to 19.0 mm. The height of the defect ranged from 5.1 to 6.1 mm. The defect was bicortical (removing the entire width of the superior margin, including the superior buccal and lingual cortical plates). In the first animal, the defect was created anterior to the mental foramen and posterior to the incisors. It was discovered that this anterior location limited the length of potential defect due to the incisor roots and also resulted in a high amount of tension on the defect. Therefore, the defects in the remaining five animals were created posterior to the mental foramen and anterior to the roots of the molars. PBSMs were trimmed under irrigation during surgery using the removed bone as a template to ensure good fit and preservation of the native anatomical planes (Fig. 6*B*). PBSMs were fixed in place within the defect by surgical plating (Fig. 6*C*). All six sheep tolerated the implantation procedure well and resumed a normal solid diet the following day with no clinical signs of discomfort or pain upon mastication.

Mandibular Reconstruction Outcomes. After 9 wk of implantation, the PBSMs were removed and the mandibles were definitively repaired in the second stage of surgery using AG bioreactor-generated tissues engineered as bony free tissue flaps. At the time of reconstruction, all six sheep were noted to have no signs of dehiscence of the PBSM. In fact, the space maintainers had successfully preserved the bony defect with soft tissue growth over the PBSM (Fig. 6*D* and *SI Appendix*, Fig. S2). Retrieval of the PBSM was easily accomplished by removing the surgical screws with minimal disturbance to soft tissue around the defect. After space maintainer harvest and fixation, soft tissue was observed to have become incorporated within the pores and along the surface of the retrieved devices (*SI Appendix*, Fig. S2 *A* and *B*). Histology showed fibrovascular tissue (*SI Appendix*, Fig. S2*C*). In the place of the preserved defect space, tissues generated from in vivo bioreactors were transferred for definitive mandibular reconstruction.

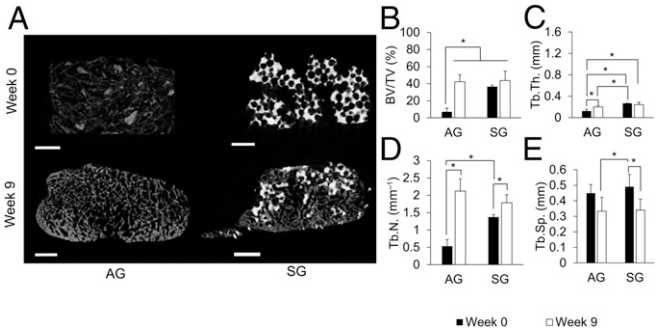

Fig. 3. Bioreactor-generated tissue radiographic studies. (*A*) Reconstructed cross-sectional images of bioreactors initially filled with AG (*Left*) or SG (*Right*) preimplantation (*Top*) and postimplantation (*Bottom*) for 9 wk against the periosteum. (Scale bars: 2 mm.) (*B–E*) BV/TV, Tb.Th., Tb.N., and Tb.Sp. AG ($n = 6$) and SG ($n = 8$) were used. Error bars represent SD. An asterisk indicates statistically significant differences (*$P < 0.05$).

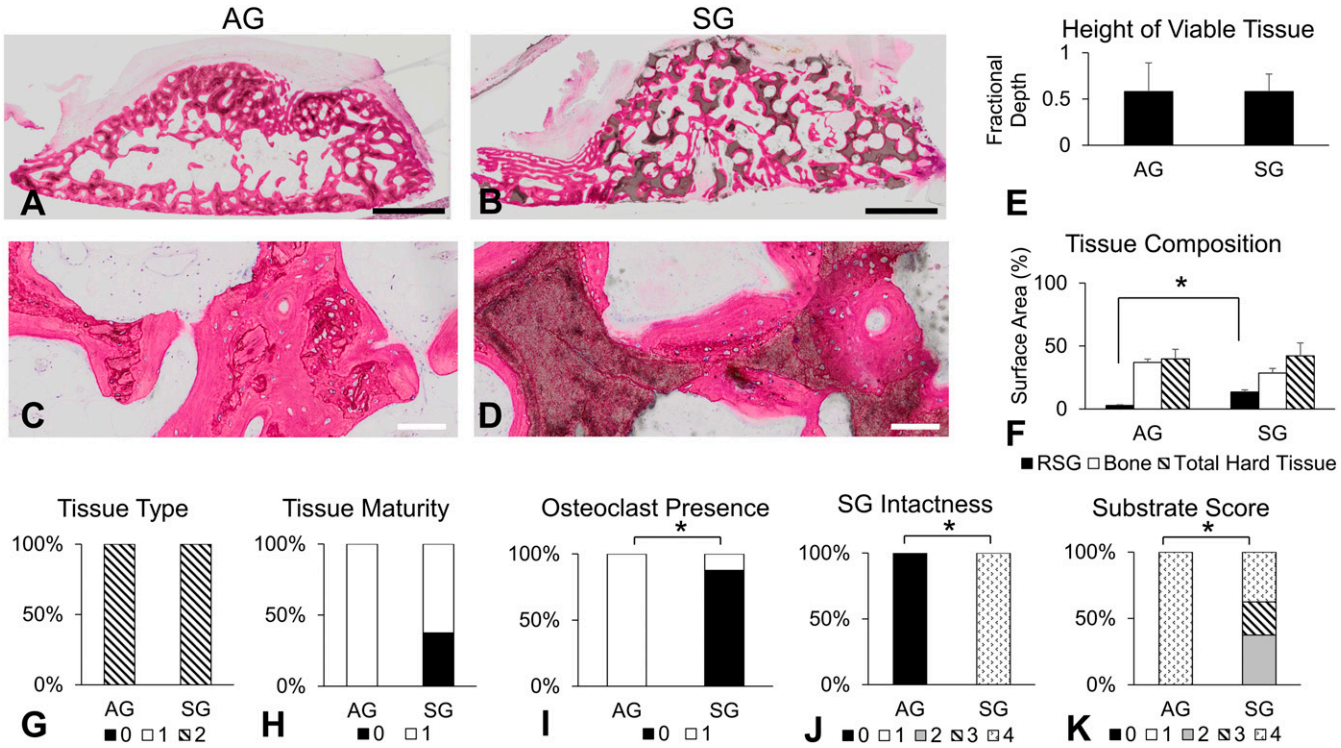

Fig. 4. Bioreactor-generated tissue histological studies. (*A–D*) Representative histological photographs at low magnification (*Top*) and high magnification (*Bottom*) of AG (*Left*) and SG (*Right*) bioreactors. (Scale bars: *Top*, 2 mm; *Bottom*, 100 μm.) (*E*) Fractional depth measurements. (*F*) Surface area (%) of remaining SG (RSG), bone, and total hard tissue (RSG + bone). (*G–K*) Histological scoring results (score correlation is shown in *SI Appendix*, Table S2). An asterisk indicates statistically significant differences (*$P < 0.05$). Error bars represent SD. AG ($n = 6$) and SG ($n = 8$) were used for all histological studies.

Mineralized tissues from AG bioreactors were harvested with their vascular pedicle intact (Fig. 6*E*). If the bioreactor-generated tissue was larger than the defect, it was trimmed to size using the PBSM as a template. This engineered bony free tissue flap was then transferred to the defect using the same surgical plate as the PBSM and screwed into place after successful anastomoses of the artery and vein with local facial vasculature (Fig. 6*F*). In sheep 2 and 3, anastomoses were unsuccessful due to lack of available facial vasculature suitable for anastomosis, so tissue was transferred as an avascular graft in these animals. All bioreactor-generated tissues were sufficiently mineralized to hold surgical screws successfully. All sheep resumed a normal diet the day following surgery.

Several days following surgery, sheep 3 and 5 were observed to have moderate swelling and erythema at the surgical site, including purulent discharge. These animals were given an additional course of postoperative enrofloxacin. Sheep 5 was initially noted to have a poor appetite. Within 4 d of treatment, both sheep had resolution of symptoms and regained a normal appetite. The other four sheep tolerated the reconstruction procedure well with no complications.

Twelve weeks after definitive reconstruction (21 wk after the initial defect creation and PBSM implantation), animals were killed and the mandibles were harvested for analysis. The oral mucosa overlying the diastema and repair site was healthy and intact in four animals. However, there was a large mucosal dehiscence over the superior and buccal surfaces of the diastema with protruding bone in sheep 5. A small defect was noted on the superior surface of the oral mucosa with no protruding bone in sheep 6. Surgical photographs are shown in *SI Appendix*, Fig. S3. Neither sheep 5 nor sheep 6 had lost a significant amount of weight, and neither sheep had any observed loss of appetite or clinical signs of pain/discomfort in the 11 wk preceding killing.

Evolution of the Density of Tissues Generated in in Vivo Bioreactors Postreconstruction. The diastemas were scanned to evaluate the mandibulocortex of the superior marginal mandible after reconstruction ("week 21," referring to the total duration of implantation of the initial biomaterial-based scaffold) compared with native mandibulocortex (contralateral side). Sheep 1 was excluded from this analysis as the defect was more anterior than in the other animals [week 21 ($n = 5$) and native ($n = 5$)]. Radiographic views facing the buccal side, superior side, and cross-section through the diastema, including the superior marginal

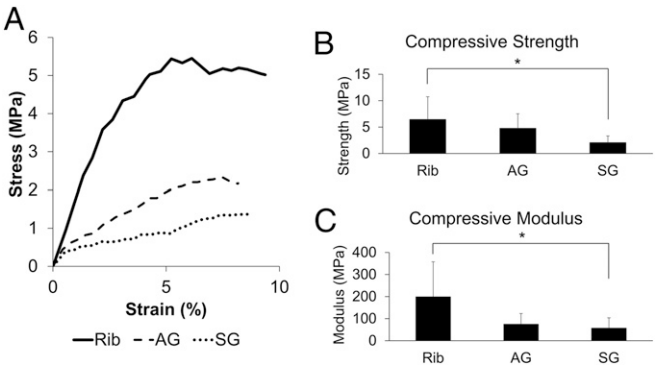

Fig. 5. Bioreactor-generated tissue mechanical studies. (*A*) Representative stress/strain graphs of rib (solid line), tissue generated from AG bioreactors (dashed line), and tissue generated from SG bioreactors (dotted line). (*B* and *C*) Compressive strength and modulus. An asterisk indicates statistically significant differences (*$P < 0.05$). Error bars represent SD. Rib ($n = 6$), AG ($n = 4$), and SG ($n = 8$) were used for determination of compressive strength. Rib ($n = 6$), AG ($n = 6$), and SG ($n = 8$) were used for determination of compressive modulus.

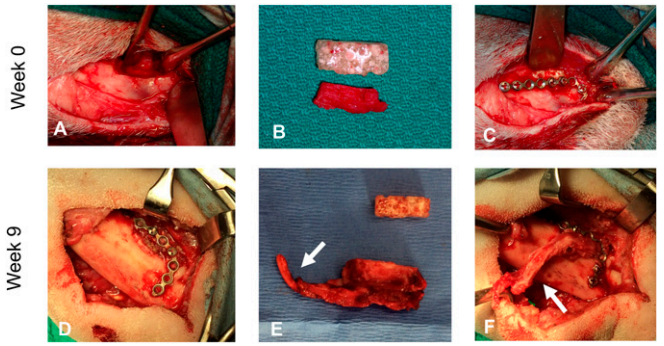

Fig. 6. Surgical photographs at the time of defect creation at week 0 (above) and at the time of defect repair at week 9 (below). (*A*) Superior marginal defect of ~20 mm in length and ~5 mm in height was created. (*B*) PBSMs were prepared during surgery based on the anatomy of each defect. (*C*) PBSM was fixed into the defect site by surgical plating. (*D*) Nine weeks after implantation, the PBSM had continued to preserve the defect site with no dehiscence and was removed for definitive reconstruction using bioreactor-generated tissues. (*E*) Removed PBSM (*Top*) and bioreactor-generated bony free tissue flap (*Bottom*) with a vascular pedicle (arrow). (*F*) Transfer of the bioreactor-generated bony free tissue flap with anastomosis of the pedicle (arrow) into the defect site to complete the mandibular repair.

area, can be viewed in Fig. 7*A* of a representative hemimandible postreconstruction and contralateral native hemimandible.

Bone within the reconstructed hemimandibles was analyzed by microcomputed tomography (microCT) by the same parameters used to analyze the bioreactor-generated tissues, as had been performed previously (6). Comparing hemimandibles postreconstruction with native hemimandibles, Tb.Th. was significantly decreased (0.72 ± 0.20 mm vs. 1.18 ± 0.19 mm, respectively); hemimandibles postreconstruction and native hemimandibles had similar BV/TV (90.55 ± 8.87% and 99.47 ± 0.38%, respectively), Tb.N. (1.34 ± 0.37 mm^{-1} and 0.87 ± 0.13 mm^{-1}, respectively), and Tb.Sp. (0.18 ± 0.06 mm and 0.12 ± 0.07 mm, respectively) (Fig. 7 *B–E*).

By comparing the radiographic data from the bioreactors preimplantation (week 0) and postimplantation (week 9) with the postreconstruction hemimandible (week 21) repaired using the tissue generated within the bioreactor, the evolution of the in vivo bioreactor-generated tissue can be followed from initial scaffold material to 21 wk after implantation within the sheep. From week 0 to week 21, the tissue significantly increased in BV/TV (Fig. 7*B*). Tb.Th. increased from week 9 to week 21 (after transfer of the bioreactor-generated tissue from the bioreactor to the mandibular defect) (Fig. 7*C*). Tb.N. significantly increased from week 0 to week 9 and then significantly decreased by week 21, reaching native Tb.N. (Fig. 7*D*). Tb.Sp. significantly decreased from week 9 to week 21 (Fig. 7*E*).

Structure of Reconstructed Hemimandibles. Sections prepared from mandibular specimens were prepared and analyzed by histomorphometry and histological scoring to better understand changes to mandibular bone size and volume postreconstruction, as well as hemimandible bridging, hardware osteointegration, and periosteal reaction postreconstruction (Fig. 8). In addition, hemimandibles were examined at high magnification for signs of acute inflammation, such as infiltrates of inflammatory cells, but no inflammation was observed (*SI Appendix*, Fig. S4).

Sheep 1 was excluded as the defect was created in a different anatomical site than the other animals [postreconstruction ($n = 5$)

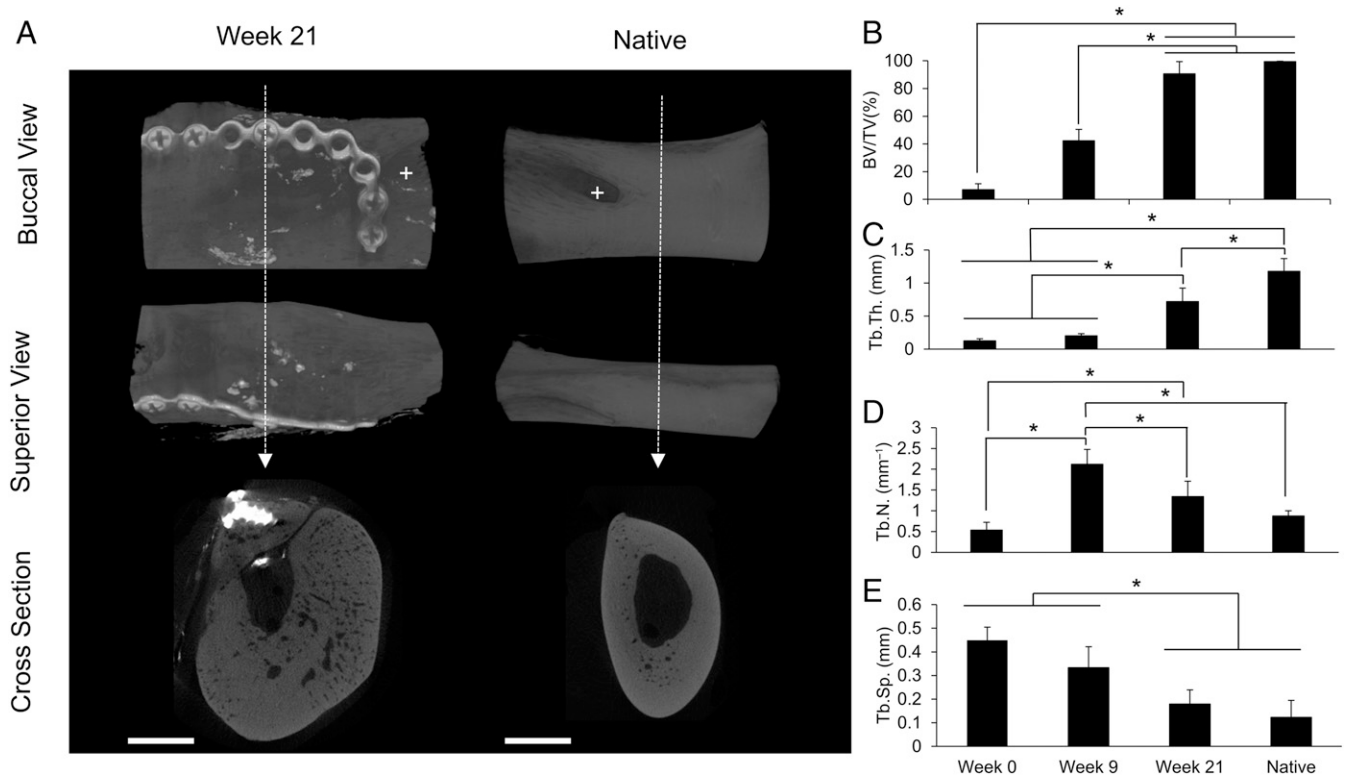

Fig. 7. Mandibular radiological studies. (*A*) Representative reconstructions of hemimandibles postreconstruction (*Left*) and the contralateral native mandible (*Right*). Buccal (*Top*), superior (*Middle*), and cross-sectional (*Bottom*) views are shown. The dotted arrow refers to the site of cross-section. (Scale bar: 5 mm.) +, mental foramen. (*B–E*) BV/TV, Tb.Th., Tb.N., and Tb.Sp [week 0 ($n = 6$), week 9 ($n = 6$), week 21 ($n = 5$), and native ($n = 5$); *x* axis shared]. Week 0 and week 9 groups are the same as those shown in Fig. 3. Error bars represent SD. An asterisk indicates statistically significant differences (*$P < 0.05$).

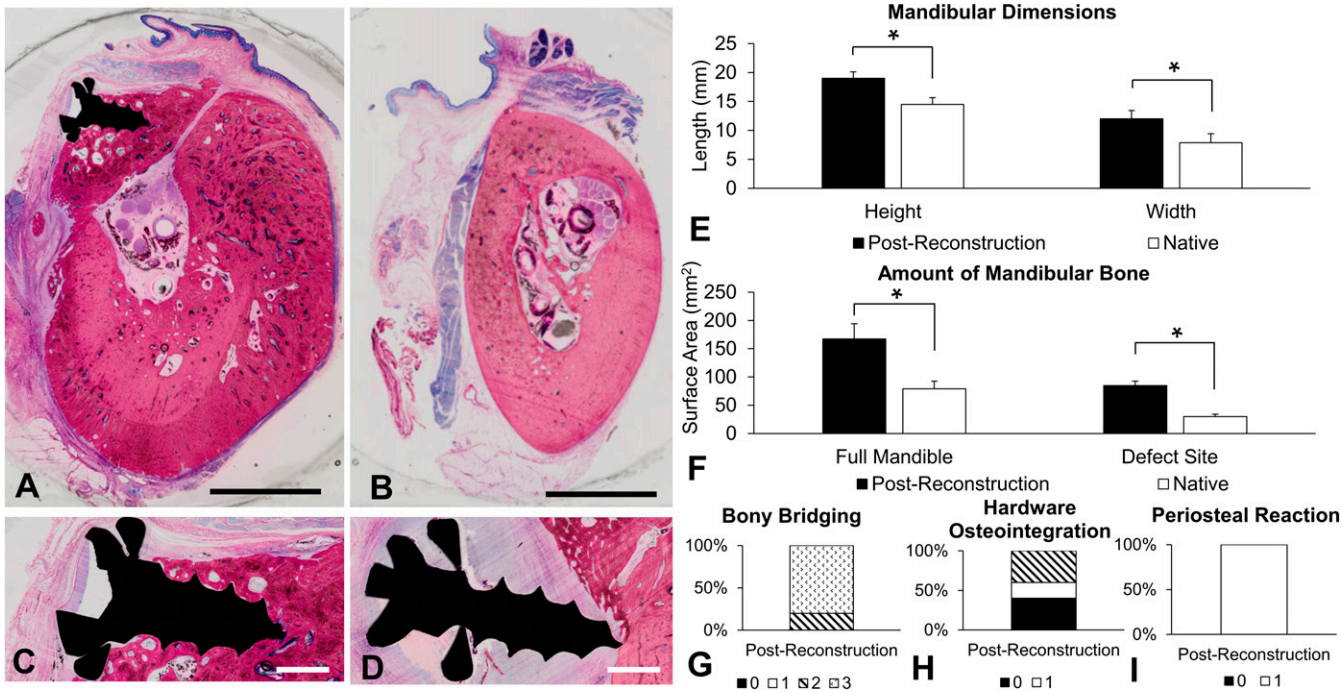

Fig. 8. Mandibular histological studies. A hemimandible postreconstruction (*A*) and a native hemimandible (*B*) are shown. (Scale bars: 5 mm.) (*C*) Example of a fully integrated screw and (*D*) a screw without osteointegration. (Scale bars: 1 mm.) (*E*) Length of hemimandibular height and width. (*F*) Surface area of bone in the full hemimandible cross-section and surface area of bone within the superior margin (defect site). (*G–I*) Histological scoring of bony bridging, hardware osteointegration, and periosteal reaction (score correlation is shown in *SI Appendix*, Table S5) [week 21 ($n = 5$) and native ($n = 5$) for all histological studies]. An asterisk indicates statistical significance (*$P < 0.05$). Error bars represent SD.

and native ($n = 5$)]. Hemimandibles postreconstruction compared with native hemimandibles had significantly greater height (18.99 ± 1.13 mm vs. 14.49 ± 1.16 mm, respectively) and greater width (11.98 ± 1.44 mm vs. 7.87 ± 1.54 mm, respectively) (Fig. 8*E*). The bony surface area in the full diastema cross-section was significantly greater in hemimandibles postreconstruction compared with native hemimandibles (167.29 ± 26.88 mm^2 vs. 79.11 ± 13.55 mm^2, respectively), as was the bony surface area in the defect site at the superior margin of the diastema (84.89 ± 7.80 mm^2 vs. 29.88 ± 4.13 mm^2, respectively) (Fig. 8*F*). Histological scoring (*SI Appendix*, Table S5) included bony bridging of the defect, integration of the screws with the tissue, and the presence of a periosteal reaction. Hemimandibles postreconstruction had >75% defect bridging in 80% of animals (Fig. 8*G*), partial or full integration of hardware in 60% of animals (Fig. 8*H*), and evidence of periosteal reaction in 100% of animals (Fig. 8*I*). These histological scores were not relevant to the contralateral native hemimandibles.

The hemimandibles featuring dehiscence were included in both histological and radiological analyses. Histological and radiographic images from the hemimandible with the largest dehiscence are shown in *SI Appendix*, Fig. S5; fibrous tissue separated the flap from the remaining native bone, and the flap no longer appeared to be viable based on osteocyte appearance. In addition, mucosa could be observed underneath a section of the flap rather than over the flap.

Discussion

The current state-of-the-art treatment for large mandibular defects, the fibula flap, is limited by the size and shape of the donor tissue. Therefore, we have developed a strategy in which engineered autologous flaps with customizable dimensions can be generated using the periosteum of the rib (5, 6). In this study, we leveraged advances in biomaterials (3D printing and porous space maintenance technology) to (*i*) three-dimensionally print bioreactors with geometry and volume conforming to a mandibular defect and (*ii*) maintain the defect space and promote healthy soft tissue envelope formation during the period of time in which tissues can be generated from in vivo bioreactors for definitive reconstruction. This strategy was applied in a challenging mandibular defect located adjacent to the oral mucosa along the superior margin of the sheep diastema (Fig. 6*A*).

In total, 83.3% of the implanted bioreactors generated mineralized tissue suitable for transfer, an improvement compared with previous recent ovine bioreactor studies [50.0% (6) and 76.9% (5)]. By radiographic analysis, both biomaterials (synthetic beta-tricalcium phosphate/hydroxyapatite composite and morcellized AG) demonstrated significant changes in Tb.N. after 9 wk of implantation within in vivo bioreactors, suggesting both materials were capable of being remodeled by cells migrating from the adjacent periosteum (Fig. 3). For the samples initially filled with morcellized AG, other parameters, including BV/TV and Tb.Th., were also significantly increased after 9 wk of implantation, while these characteristics did not significantly increase for samples initially filled with SG, perhaps suggesting that morcellized AG was more readily remodeled than SG. There were no significant differences in final tissue density, Tb.Th., Tb.N., or Tb.Sp. between tissues generated in bioreactors between either scaffold group despite significant differences before implantation. These final radiological parameters are similar to those reported previously in tissues generated from the ovine in vivo bioreactor model (6). Compared with microCT values reported in the literature regarding native sheep trabecular bone (22), tissues generated from the in vivo bioreactor have greater BV/TV, suggesting that the bone may be corticocancellous in nature rather than strictly trabecular.

Histologically, tissues generated from AG had more osteoclasts present (a marker indicating greater bone maturity) and

had greater substrate scores (Fig. 4). These differences in bone maturity and scaffold encapsulation may be attributed to the additional osteogenic growth factors present in morcellized AG (23). In prior ovine in vivo bioreactor studies, denaturing proteins in morcellized AG via autoclave before implantation resulted in significantly decreased bony tissue generation (24). Likewise, using synthetic polymer scaffolds with no inherent osteoconductive or osteoinductive properties significantly decreased bony tissue generation (25). While not inherently containing any growth factors or cell recognition motifs, synthetic bioceramics have generated viable bone tissue of similar height and density to autologous bone grafts in the ovine bioreactor model (5, 6). It has been hypothesized that this effect may be attributed to the rapid degradation of the tricalcium phosphate portion of the ceramic resulting in locally elevated concentrations of calcium and phosphate ions, promoting osteogenic differentiation of progenitor cells (26). In this study, the height of viable bone produced and amount of bony surface area and total mineralized tissue surface area were not different between groups (Fig. 4 *E* and *F*), as had been observed previously (5, 6).

Mechanical studies are important in evaluating bone tissue engineering strategies as they address the functional status of tissue constructs. In this study, bioreactor-generated tissues were transferred to a mandibular defect site that experiences mechanical loading adjacent to the oral mucosa in comparison to past studies in nonloaded mandibular angle defects (5, 6). Consistent with histological studies, compressive strength and modulus measurements suggested that AG was more mature and similar to native rib bone compared with SG groups (Fig. 5). In a prior porcine model, decellularized bovine bone was used as a scaffold to generate tissues from in vivo bioreactors (27). The resulting compressive strength of bioreactor-generated tissue was found to be similar to that of native mandibular bone, and thus speculated to be sufficient for repair (27). Comparing results, both the AG and SG tissues in this study have higher compressive strength than tissues reported from the porcine in vivo bioreactor.

Biomolecular assays of gene expression demonstrated similar expression of osteogenic, chondrogenic, and angiogenic markers among AG and SG groups (*SI Appendix*, Fig. S6 and Table S6), as has previously been noted in the ovine in vivo bioreactor model (6). As these genes are less highly expressed in mature bone tissue (28), it is possible that significance was not observed due to the time point at which the tissues were biopsied.

AG is the gold standard scaffold material for bony reconstruction (21), and therefore was chosen as the scaffold of choice for mandibular reconstruction. Nevertheless, harvesting AG increases the risk of donor site morbidity in clinical practice (3). The use of SG eliminates the need for harvest of autologous bone to generate AG and would ultimately reduce donor site morbidity, a major challenge in the field of reconstruction. When designing this study, data from a prior head-to-head ovine bioreactor study comparing the same two biomaterials were taken into consideration and demonstrated significantly increased BV/TV, Tb.N., and bone surface area in tissues generated from bioreactors with AG compared with SG (6). Given that the chosen mandibular defect was significantly more rigorous than those studied previously (5, 6), AG was selected as the biomaterial to optimize bioreactor-generated tissue properties as much as possible before transfer into the defect. However, given the success of this study and the exciting clinical advantages to minimizing the use of autologous tissues, future work will study the transfer of tissues generated from only synthetic materials for mandibular reconstruction. While tissues generated from SG bioreactors may be less mature per histological and mechanical analysis, data suggest that transfer of tissues from SG bioreactors to mandibular defects results in further tissue maturation after transfer (6). Alternatively, SG may be mixed with AG (6) to reduce the volume of autologous bone required and minimize the risk of donor site morbidity.

It has previously been demonstrated that vascularized free flaps are appropriate for reconstructing mandibular defects and are superior to nonvascularized grafts (1). Therefore, while a group involving autologous tissue (either as a vascularized flap or as a nonvascularized graft) could have served as a control in this study, we sought to reduce the number of animals needed in collaboration with our veterinarian colleagues, as prior studies have examined mandibular reconstruction with autologous tissue in sheep (29–31).

Unlike prior in vivo bioreactor studies in the ovine model featuring mandibular reconstruction, this study included defect creation during the first stage of surgery rather than the second stage of surgery so as to model clinical scenarios more realistically (5, 6). In addition, porous space maintainers were inserted into the defect site to optimize soft tissue growth as well as prevent scar tissue from distorting the defect before definitive repair, as has been done in human cases (15, 17). All animals tolerated defect creation and implantation of the PBSMs well. While current human protocols regarding mandibular surgery recommend a liquid diet following operations, these animals were permitted to resume their normal diet (hard pellet food and hay) the day following surgery. Although this could have disrupted the vulnerable oral mucosa overlying the porous space maintainers, none of the sheep demonstrated soft tissue dehiscence over the space maintainers at the time of the second surgical procedure (9 wk after implantation). In fact, soft tissue had integrated well with the porous space maintainers, filling superficial pores and covering sections of the spacer surface (*SI Appendix*, Fig. S2). It has been shown that porous space maintainers are less likely to be associated with dehiscence compared with solid space maintainers (15); although this study was not designed to compare solid versus porous space maintenance, it is possible that this porosity prevented dehiscence of the oral mucosa during the space maintenance phase.

In previous ovine in vivo bioreactor studies, the mandibular defect was located at the angle of the mandible (5, 6). This anatomical site is not subjected to biomechanical load, is not adjacent to the oral mucosa, and is located near the major vessels of the neck for ease of anastomoses during tissue transfer. In the more rigorous superior marginal defect created in the diastema during this study, vascular access was more challenging. In two animals, anastomosis was unsuccessful and the tissues were implanted as avascular grafts. A previous ovine study indicated that there was not a significant difference between transfer of bioreactor-generated tissues as avascular grafts or vascularized flaps when transferring tissues generated from bioreactors with SG (6). AG and SG tissues may not be directly comparable; however, given that SG tissues have been shown to be less mature at the time of transfer, it may be possible that they would be expected to be even more vulnerable to necrosis from lack of vasculature. In addition to the transferred group, the current model differs from prior work due to the defect site at a load-bearing location with proximity to the oral mucosa and different vascular access. Despite this rigorous defect, the clinical outcomes for the two animals receiving avascular grafts rather than vascularized flaps demonstrated no apparent disadvantage relative to the animals whose bioreactor vascular pedicles were feasibly anastomosed to facial vasculature. Future studies will better characterize vascularization in these transferred tissues with and without anastomoses and as a function of the initial bioreactor scaffold.

Following definitive reconstruction, all animals immediately resumed a normal diet (hard pellet food and hay). In human patients, a liquid diet with transition to a soft food diet would be strongly recommended in the weeks following reconstruction to prevent biomechanical trauma from disrupting the transferred

tissue as it osteointegrates with the adjacent native bone. In fact, failure in a well-documented human case of mandibular reconstruction using an in vivo bioreactor strategy was attributed to dehiscence caused by the patient eating hard foods against medical advice. In that case, mucosal dehiscence was followed by infection and eventual loss of the tissue-engineered reconstructed graft (32). In the present study, at the time of killing, one animal had a large dehiscence of the oral mucosa over the transferred tissue (*SI Appendix*, Figs. S3*B* and S5). While a suboptimal surgical outcome, the animal did not demonstrate any clinical signs of discomfort or weight loss between resolution of infection and killing (~11 wk), so this event was not considered catastrophic. This sheep was still included in subsequent radiological and histological analysis. In addition to this large tissue dehiscence, another mandible had a small dehiscence noted as well. In humans, small mucosal dehiscences occurring over mandibles reconstructed using flaps can self-resolve by secondary intention (33). As there were no radiological signs of resorption or flap failure, this animal was regarded as having a successful surgical outcome. Of note, although sheep 1 could not be compared radiologically and histologically with sheep 2–6 due to a different defect site placement (anterior to the mental foramen), there were no noted dehiscences, and there was reasonable evidence of osteointegration with surrounding tissues and a successful surgical outcome.

Radiographically, 12 wk after transfer to the mandibular defect, bioreactor-generated tissues continued to mature and evolve in density and structure according to microCT measurements (Fig. 7 *B*–*E*). This is consistent with prior findings with SG bioreactor-generated tissues (6). It had previously been observed that when placed in bioreactors against the sheep periosteum for over 12 wk, bioreactor-generated tissues actively became demineralized (24). It was speculated that this was due to lack of biomechanical stimulation within the bioreactors at later time points. By transferring the tissue to a superior marginal defect, the tissue experienced forces associated with mastication due to its proximity to the oral mucosa (although as an edentulous area, less force than the mandibular bone supporting the incisors or molars). This stimulation, in combination with environmental factors local to the defect site, may be responsible for the continuing maturation of the bioreactor-generated tissue postreconstruction.

Histologically, bony bridging and partial-to-full hardware osteointegration occurred in the majority of hemimandibles postreconstruction (Fig. 8 *G* and *H*). Lack of mandibular hardware osteointegration has been observed by multiple groups in ovine studies and has been speculated to be due to the lateral mastication motion of ruminants (34, 35). Signs of a periosteal reaction, an inflammatory response in response to disruption of the periosteum, were observed in all of the reconstructed hemimandibles (Fig. 8*I*). The periosteal reaction is particularly robust in sheep and ruminants in general (34). While it is generally thought that the excess bone from the periosteal reaction resorbs over time, it has been shown to persist for at least 24 wk postsurgery in a sheep study (34). Given that the final dimensions of the hemimandible postreconstruction are larger than the native mandible, the increased mandibular width, height, and bony volume are most likely attributed to both the transferred bioreactor-generated tissue and the periosteal reaction (Fig. 8 *E* and *F*). Given that the study was not designed to determine the extent of periosteal reaction in the healing of the defect alone, it is difficult to separate out these factors. However, it is of note that other ovine mandibular defect models of similar duration have been shown not to heal within 12 wk without further intervention (35), suggesting that the periosteal reaction alone would not have been sufficient for the degree of postreconstruction regeneration observed in this study. In addition to the periosteal reaction, it is possible that other sources of inflammation could have caused additional bony growth. No acute signs of inflammation were observed at week 21 (*SI Appendix*, Fig. S4). However, as there were no time points taken between mandibular reconstruction and mandible harvest [a 12-wk period has previously been shown to be sufficient to demonstrate osteointegration in the mandible in the sheep model (5, 6)], it is possible that other inflammatory processes may have occurred and the acute phase may have resolved by our terminal time point. Additional time points in future studies may offer more insight into the integration and remodeling process of the transferred bioreactor-generated tissue.

In this work, a combination of porous space maintenance and 3D-printed in vivo bioreactors was used to reconstruct a mandibular defect in a large animal model. A total of 20 of 24 bioreactors generated tissues appropriate for reconstruction. While both SG and AG scaffolds were capable of supporting the generation of mineralized tissue conforming to the size and shape of the implanted bioreactors, AG generated more mature bone tissue with mechanical properties more similar to native bone. Space maintainers integrated well with local soft tissue and successfully preserved a superior marginal bony defect in the ovine diastema during the generation of autologous vascularized bone free tissue flaps of custom geometry from 3D-printed in vivo bioreactors implanted against the periosteum of the rib. Overall, the surgical outcome was satisfactory in the reconstruction of five of six mandibular defects in a large animal model.

Materials and Methods

Bioreactor and Porous Space Maintainer Fabrication. Bioreactors were printed from PMMA using a layer-by-layer technique to print hollow rectangular blocks with one open face and inner dimensions of 2 cm in length, 1 cm in width, and 0.5 cm in height. A sheet of ethylene-vinyl acetate was formed around each bioreactor to create a cuff capable of holding suture with ~0.5 cm of overhang on each edge of the bioreactor. Bioreactors were sterilized by exposure to ethylene oxide gas.

Porous space maintainers were fabricated from PMMA and carboxymethylcellulose gel as previously described (12, 36, 37) using reagents prepared by Synthasome, Inc. Briefly, 7% (wt/vol) carboxymethyl cellulose was added to a bone cement powder phase consisting of polymerized methylmethacrylate/methacrylate copolymer, benzyl peroxide, and zirconium dioxide at a ratio of 30:70 carboxymethylcellulose/bone cement powder phase (wt/wt). The bone cement liquid phase, consisting of methacrylate monomer, *N*,*N*-dimethyl-4-toluidine, and hydroquinone, was added at a ratio of 2.12:2 powder phase/liquid phase (wt/wt). The mixture was stirred until doughing, at which point it was placed into a polytetrafluoroethylene mold in the shape of a human mandible and allowed to cure for at least 24 h. The space maintainers were sterilized by electron beam irradiation (Sterigenics International LLC) (36). Blocks were cut to the size of the intended sheep mandibular defect under sterile conditions by a diamond blade saw (South Bay Technologies) and stored under sterile conditions until implantation.

Bioreactor and Space Maintainer Implantation. All animal use was approved by the Animal Welfare Committee of the University of Texas Health Science Center and Animal Care and Use Review Office of the US Department of Defense. Six female Dorper sheep (supplied by William Edmiston, Eldorado, TX), aged 4–6 mo and weighing 40.4 ± 7.3 kg on average, were anesthetized, prepared, and intubated. Anesthesia was performed using inhaled isoflurane (3–5% for induction and 1.5–3% for maintenance) and i.v. Telazol (2–8 mg/kg), with the level of anesthesia monitored via lack of palpebral (blink) reflex, lack of toe/tail pinch reflex, and changes in cardiopulmonary parameters (heart rate, respiratory rate, and blood pressure). Additional analgesia included fentanyl patches (75–100 μg per 45 kg), intramuscular ketoprofen (2–3 mg/kg), intramuscular buprenorphine (0.005–0.01 mg/kg), and local bupivacaine (0.25%) at incision sites. Two incisions of up to 15 cm in length were made on the right flank over the rib cage. After periosteal dissection, bony segments of 3–4 cm in length were harvested from the second, fourth, sixth, and eighth ribs. Pieces of these segments were morcellized to create AG. Bioreactors were filled with AG or SG (MASTERGRAFT Granules, Medtronic; composition of 85% beta-tricalcium phosphate/15% hydroxyapatite, average diameter of 1.6–3.2 mm, porosity of 80%, and average pore size of 500 μm as reported by the manufacturer). The bioreactors implanted on the second and fourth ribs were consistently AG-filled bioreactors. The sixth rib was always implanted with an SG-filled bioreactor. The eighth rib was randomized to be implanted with either an AG- or SG-filled

bioreactor (n = 3 and n = 3, respectively). As the mandibular defect was always reconstructed with tissue from an AG-filled bioreactor, and hence one AG-filled bioreactor per animal was unavailable for analysis, this approach allowed for an equal number of potential AG- and SG-filled bioreactor-generated tissues for analysis (n = 9 per scaffold type). Bioreactors were secured by suturing the cuff to the periosteum such that the open face of the bioreactor was in communication with the cambium layer of the periosteum. After bioreactor implantation, the incisions were closed.

Simultaneous to bioreactor implantation, a second surgical team performed a mandibular resection and implantation of the PBSM. An incision of up to 4 cm was made along the inferior border of the right hemimandible at the diastema (the edentulous region of the sheep mandible). The superior border of the diastema was exposed, and a defect of up to 2 cm in length was created by a burr (NSK Surgery). The resection included both the buccal and lingual plates. The PBSM was trimmed by surgical burr under irrigation to match the dimensions of the resected bone. The PBSM was secured into the defect by a titanium midface plate (KLS Martin) with two self-tapping titanium screws holding the space maintainer and two additional screws on either side of the defect holding the plate to the native mandible. After irrigation, the mandibular incision was closed.

Mandibular Reconstruction and Bioreactor Tissue Harvest. Nine weeks following implantation of the bioreactors and PBSM, the mandible was definitively repaired using tissue generated from AG bioreactors. Briefly, under general anesthesia, bioreactors were located through two incisions of up to 15 cm in length along the right flank of the rib cage. The AG bioreactor on the second rib was always used for transfer, with the AG bioreactor implanted on the fourth rib as a suitable second option depending on the availability of viable vasculature for anastomoses and in the event that mineralized tissue was not formed within the second rib bioreactor. The remaining bioreactors, as well as recovered PBSMs, were harvested without vasculature for subsequent fixation and radiographic analysis. The PBSM was removed with an effort made to minimally disrupt any soft tissue surrounding the implant. Tissues were fixed in 10% neutral buffered formalin for 1 wk and then stored at 4 °C in 70% ethanol. The chest incisions were closed after the harvest of all four bioreactors.

The mandible was reexposed using the same approach as in the first surgical procedure. The PBSM was then removed from the defect. In its place, an engineered bone free tissue flap generated from AG bioreactors was implanted along the same titanium midface plate using one to two titanium self-tapping screws (KLS Martin). Vascular anastomoses were performed with the aid of a surgical microscope (Leica Microsystems); the intercostal artery and vein were harvested with the free flap and joined by side-to-side and end-to-side orientation with branches of the facial artery and vein, with confirmation of patency by observation of arterial pulsations.

Mandibular Harvest. Twelve weeks following reconstruction of the mandible, animals were killed and the entire mandible was harvested. Briefly, animals were killed by i.v. administration of an entobarbital/phenytoin mixture. The skin was dissected from the mandible with care to preserve the oral mucosa. Mandibles were harvested by dissection of attached tendons and ligaments, and then removal of the condyles from the temporomandibular joint. Mandibles were cleaved into hemimandibles using a diamond blade. The diastema was then isolated by diamond blade saw, fixed for 1 wk, and stored in 70% ethanol at 4 °C.

Radiological Studies. Bioreactor and mandibular specimens were subjected to microCT using a SkyScan 1172 microCT imaging system as previously described (5, 6). Briefly, specimens were scanned with an X-ray source of 59 kV and current of 167 μA with an aluminum/copper filter at a voxel size of 17.1 μm. Using NRecon (version 1.6.9.18; SkyScan), reconstruction was performed with a threshold of 0.002–0.116 (dimensionless) (6). To measure the quantity and quality of mineralized tissue, reconstructed images were analyzed using CTAn (version 1.15.4.0; SkyScan).

For analysis of tissue specimens generated from in vivo bioreactors, BV/TV, Tb.Th., Tb.N., and Tb.Sp. were measured. Briefly, a region of interest (ROI) was selected for each bioreactor specimen such that it did not overlap with the void space outside of the edges of the specimen. The ROIs were converted to binary scale, and a binary threshold of 40–255 (dimensionless) was applied to select mineralized tissue. In addition to specimens harvested from bioreactors after 9 wk of implantation, bioreactors filled with SG (n = 6) and bioreactors filled with AG from harvested rib (n = 6, one rib per animal) were scanned before implantation (week 0).

For analysis of mandibular specimens, the right-sided (reconstructed) mandibular diastema (week 21) and left-sided contralateral (native) mandibular diastema were also analyzed for BV/TV, Tb.Th., Tb.N, and Tb.Sp. An ROI was selected within the reconstructed defect region at the superior border of the diastema, superior to the inferior alveolar canal and medial to the screws and plates implanted along the buccal surface of the mandible.

Histological Studies. Following microCT scanning, bioreactor-generated specimens were cut in half by a diamond blade saw; in randomized fashion, one half was analyzed by histology and the other half underwent mechanical testing. All mandibles underwent histological evaluation. Briefly, specimens were serially dehydrated in ethanol solutions and then embedded in PMMA as described previously (6). Specimens were sectioned into 10-μm slices by a diamond blade microtome (Leica Microsystems SP 1600) and stained with methylene blue/basic fuchsin.

Sections from bioreactor-generated tissues and PBSMs were taken at midpoint of the length of the total specimen (the edge of the specimen after being cut in half). Sections from the diastema were captured through and between the anterior and posterior screws, ensuring that the captured tissues were within the site of the initial defect. Three to four sections were made from each specimen. Images of sections were taken with a BX51 Olympus Slidescanner (Olympus Corporation).

Sections from each bioreactor-generated tissue specimen (n = 3 per specimen) were scored in randomized order by three blinded independent reviewers (E.W., T.C.P., and B.T.S.) using a previously described histological scoring system (6) (*SI Appendix*, Table S2). Sections prepared from reconstructed mandibles were scored by the same blinded reviewers for hardware osteointegration, bony bridging, and presence of periosteal reaction (n = 3 per specimen) (*SI Appendix*, Table S5). The median score of the three sections per specimen was used as the final score of that specimen per guidelines for valid histological scoring (38).

Histomorphometric analysis was performed on sections from the bioreactor-generated specimens (n = 3 per specimen) as well as hemimandibles postreconstruction and native hemimandibles (n = 3 per specimen) using ImageJ (NIH) based on previously described methods (5, 6). Briefly, the fractional depth of the bioreactor-generated specimens was determined by calculating the mean of the distance between the periosteum (x axis) and furthest viable osteocyte in a line perpendicular to the x axis at 1/3, 1/2, and 2/3 the length of the periosteum normalized by the height of the bioreactor (5 mm). The surface area of bone and SG as a function of the total tissue surface area in bioreactor-generated specimens was calculated by applying the same image-thresholding parameters across all specimens to select for bone and remaining SG as has been described previously (5, 6).

The width and height of the hemimandibular specimens were calculated by measuring the distance between cortical plates in a line parallel to the inferior edge of the alveolar canal and by measuring the distance from the midpoint of the inferior edge of the mandible to the superior edge of the hemimandible in a line parallel to the cortical plates. The surface area of bone in hemimandibular specimens was measured using the same threshold parameters for bone as used in the bioreactor specimens after subtracting the surface area of the screws. The defect height of each specimen was determined by measuring the corresponding height of the PBSM after being trimmed to fit within the specific defect. For each hemimandible postreconstruction, the defect area was calculated by measuring the total height of the corresponding native hemimandible (the original height before surgery), subtracting the defect height to find the native bone height, and then isolating the tissue above the native bone height. This same calculation was performed in the contralateral native hemimandible to determine the native amount of bone within the defect area. The final fractional depth, surface areas, and lengths for each specimen were taken from the mean value of the three sections corresponding to that section (39).

Mechanical Studies. Cubes were cut from fixed ribs of sheep (n = 1 per animal for a total of n = 6) and the bioreactor-generated specimen halves (n = 1 per specimen) by a diamond blade saw such that no dimension (length, width, and height) exceeded 5 mm and no aspect ratio exceeded 2:1. The soft tissue encapsulating specimens was removed when present. Specimens were subjected to mechanical testing via a Mini Bionix 858 (MTS Systems Corporation) with a 10-kN load cell under a cross-head speed of 1 mm·min^{-1} until either fracture or passing of the upper yield point. The software TestWorks 4 (MTS Systems Corporation) was used to calculate compressive strength (determined from the 2% offset load) and modulus. Specimens that failed to yield were excluded from analysis.

Biomolecular Studies. Gene expression from the soft tissue envelope of bioreactor-generated specimens was determined based on previously

described methods (6). Briefly, 3-mm biopsies of tissue were taken from the surface of the bioreactor-generated specimens adjacent to the rib periosteum (bottom or "-B") and from the surface farthest from the periosteum (top or "-T") at the time of harvest. These specimens were preserved in RNAlater (Thermo Fisher Scientific) and stored at −20 °C until processing. Tissues were then homogenized in RLT Lysis Buffer (Qiagen) with a TissueLyser II (Qiagen) and isolated using a RNeasy Kit (Qiagen). Isolated RNA was then added as a template for cDNA synthesis using VeriScript Reverse Transcriptase (Isogen Life Science). Dilutions of cDNA were made in sheared salmon sperm DNA (Thermo Fisher Scientific). Quantitative real-time PCR was then performed on a CFX96 Real-Time System (Bio-Rad) for a panel of genes and growth factors associated with angiogenesis, osteogenesis, and chondrogenesis, using primers (40–42) outlined in *SI Appendix*, Table S6, via Power SYBR Green PCR Master Mix (Thermo Fisher Scientific). Each reaction was run with 20 ng of cDNA diluted in sheared salmon sperm DNA. Glyceraldehyde 3-phosphate dehydrogenase (*GAPDH*) was employed as the housekeeping gene for data normalization. Relative mRNA expression was calculated by comparing the number of cycles required to attain a threshold fluorescence within each sample to the *GADPH* housekeeping gene ($2^{-\Delta Ct}$ method). Samples were run in duplicate and averaged to determine expression per specimen (39).

Statistics. All radiological, histomorphometric, mechanical, and biomolecular data were analyzed using one-way ANOVA with a post hoc Tukey's honestly significant difference test ($\alpha = 0.05$). Histological scoring data were analyzed using a Kruskal–Wallis test with post hoc analysis via the Steel–Dwass test. All statistics were performed using JMP Pro-11.0 (SAS).

ACKNOWLEDGMENTS. A.M.T., G.L.K., E.W., S.R.S., and B.T.S. thank the Baylor College of Medicine Medical Scientist Training Program. We acknowledge the help and support of Dr. Julia Goldman, Peggy Bek, the veterinary staff of the University of Texas Health Science Center at Houston, Natasja van Dijk, Irene Otte-Holler, Meyke Hermsen, Casey Rehfeld (KLS Martin), and Dr. Daniel Felleman. This work was supported by the Osteo Science Foundation and the NIH (Grant P41 EB023833). This work was also supported, in part, by the US Army, Navy, NIH, Air Force, and Veterans Affairs and Health Affairs to support the Armed Forces Institute of Regenerative Medicine II effort, under Award W81XWH-14-2-0004. The US Army Medical Research Acquisition Activity is the awarding and administering acquisition office. A.M.T. acknowledges the Barrow Scholars Program, and G.L.K. is supported by the Robert and Janice McNair Foundation MD/PhD Student Scholar Program. E.W. is supported by the National Institute of Dental and Craniofacial Research (Grant F31 DE027586), B.T.S. is supported by the National Institute of Arthritis and Musculoskeletal and Skin Diseases (Grant F30 AR071258), and S.R.S. is supported by the National Institute of Arthritis and Musculoskeletal and Skin Diseases (Grant F30 AR067606). Opinions, interpretations, conclusions, and recommendations are those of the authors and are not necessarily endorsed by the Department of Defense.

1. Bak M, Jacobson AS, Buchbinder D, Urken ML (2010) Contemporary reconstruction of the mandible. *Oral Oncol* 46:71–76.
2. Hayden RE, Mullin DP, Patel AK (2012) Reconstruction of the segmental mandibular defect: Current state of the art. *Curr Opin Otolaryngol Head Neck Surg* 20:231–236.
3. Schrag C, Chang YM, Tsai CY, Wei FC (2006) Complete rehabilitation of the mandible following segmental resection. *J Surg Oncol* 94:538–545.
4. Tatara AM, Wong ME, Mikos AG (2014) In vivo bioreactors for mandibular reconstruction. *J Dent Res* 93:1196–1202.
5. Tatara AM, et al. (2015) Autologously generated tissue-engineered bone flaps for reconstruction of large mandibular defects in an ovine model. *Tissue Eng Part A* 21: 1520–1528.
6. Tatara AM, et al. (2016) Reconstruction of large mandibular defects using autologous tissues generated from in vivo bioreactors. *Acta Biomater* 45:72–84.
7. Akar B, et al. (2018) Large animal models of an in vivo bioreactor for engineering vascularized bone. *Tissue Eng Part B Rev* 24:317–325.
8. Kermer C, Ziya-Ghazvini F, Poeschl PW, Klug C (2004) Two stage reconstruction with revascularized grafts after resection of retromolar and oropharyngeal carcinoma. *Int J Oral Maxillofac Surg* 33:554–557.
9. Rohner D, et al. (2003) Maxillofacial reconstruction with prefabricated osseous free flaps: A 3-year experience with 24 patients. *Plast Reconstr Surg* 112:748–757.
10. Zwetyenga N, et al. (2009) Mandibular reconstruction using induced membranes with autologous cancellous bone graft and HA-betaTCP: Animal model study and preliminary results in patients. *Int J Oral Maxillofac Surg* 38:1289–1297.
11. Goodger NM, Wang J, Smagalski GW, Hepworth B (2005) Methylmethacrylate as a space maintainer in mandibular reconstruction. *J Oral Maxillofac Surg* 63:1048–1051.
12. Henslee AM, et al. (2014) Use of porous space maintainers in staged mandibular reconstruction. *Oral Maxillofac Surg Clin North Am* 26:143–149.
13. Christou C, Oliver RA, Yu Y, Walsh WR (2014) The Masquelet technique for membrane induction and the healing of ovine critical sized segmental defects. *PLoS One* 9: e114122.
14. Gruber HE, et al. (2016) Osteogenic, stem cell and molecular characterisation of the human induced membrane from extremity bone defects. *Bone Joint Res* 5:106–115.
15. Kretlow JD, et al. (2010) Evaluation of soft tissue coverage over porous polymethylmethacrylate space maintainers within nonhealing alveolar bone defects. *Tissue Eng Part C Methods* 16:1427–1438.
16. Vaandrager JM, van Mullem PJ, de Wijn JR (1983) Porous acrylic cement for the correction of craniofacial deformities and repair of defects, animal experimentation and two years of clinical application. *Biomaterials* 4:128–130.
17. Shah SR, et al. (2016) Polymer-based local antibiotic delivery for prevention of polymicrobial infection in contaminated mandibular implants. *ACS Biomater Sci Eng* 2: 558–566.
18. Cohen A, Laviv A, Berman P, Nashef R, Abu-Tair J (2009) Mandibular reconstruction using stereolithographic 3-dimensional printing modeling technology. *Oral Surg Oral Med Oral Pathol Oral Radiol Endod* 108:661–666.
19. Rengier F, et al. (2010) 3D printing based on imaging data: Review of medical applications. *Int J CARS* 5:335–341.
20. Rana M, et al. (2011) Reconstruction of mandibular defects–Clinical retrospective research over a 10-year period. *Head Neck Oncol* 3:23.
21. Gazdag AR, Lane JM, Glaser D, Forster RA (1995) Alternatives to autogenous bone graft: Efficacy and indications. *J Am Acad Orthop Surg* 3:1–8.
22. Mittra E, Rubin C, Qin YX (2005) Interrelationship of trabecular mechanical and microstructural properties in sheep trabecular bone. *J Biomech* 38:1229–1237.
23. van der Donk S, et al. (2003) Rinsing morselized allografts improves bone and tissue ingrowth. *Clin Orthop Relat Res* 408:302–310.
24. Cheng MH, et al. (2005) Ovine model for engineering bone segments. *Tissue Eng* 11: 214–225.
25. Thomson RC, et al. (1999) Guided tissue fabrication from periosteum using preformed biodegradable polymer scaffolds. *Biomaterials* 20:2007–2018.
26. Barradas AM, et al. (2012) A calcium-induced signaling cascade leading to osteogenic differentiation of human bone marrow-derived mesenchymal stromal cells. *Biomaterials* 33:3205–3215.
27. Warnke PH, et al. (2006) The mechanical integrity of in vivo engineered heterotopic bone. *Biomaterials* 27:1081–1087.
28. Kuroda S, Virdi AS, Dai Y, Shott S, Sumner DR (2005) Patterns and localization of gene expression during intramembranous bone regeneration in the rat femoral marrow ablation model. *Calcif Tissue Int* 77:212–225.
29. Çakır-Özkan N, Eyibilen A, Özkan F, Gülbahar MY, Kabak YB (2011) Immunohistochemical analysis of reconstructed sheep mandibles: Transport distraction osteogenesis versus autogenous bone grafting. *J Oral Maxillofac Surg* 69:1248–1254.
30. Koole R, Visser WJ, Klein WR, Suiker AM (1991) A comparative investigation on autologous mandibular and iliac crest bone grafts. An experimental study in sheep. *J Craniomaxillofac Surg* 19:133–143.
31. Adeyemo WL, et al. (2008) Influence of host periosteum and recipient bed perforation on the healing of onlay mandibular bone graft: An experimental pilot study in the sheep. *Oral Maxillofac Surg* 12:19–28.
32. Warnke PH, et al. (2006) Man as living bioreactor: Fate of an exogenously prepared customized tissue-engineered mandible. *Biomaterials* 27:3163–3167.
33. Wei FC, Seah CS, Tsai YC, Liu SJ, Tsai MS (1994) Fibula osteoseptocutaneous flap for reconstruction of composite mandibular defects. *Plast Reconstr Surg* 93:294–304, discussion 305–306.
34. Kallela I, et al. (1999) Fixation of mandibular body osteotomies using biodegradable amorphous self-reinforced (70L:30DL) polylactide or metal lag screws: An experimental study in sheep. *J Craniomaxillofac Surg* 27:124–133.
35. Schouman T, Schmitt M, Adam C, Dubois G, Rouch P (2016) Influence of the overall stiffness of a load-bearing porous titanium implant on bone ingrowth in critical-size mandibular bone defects in sheep. *J Mech Behav Biomed Mater* 59:484–496.
36. Tatara AM, et al. (2015) Effects of electron beam sterilization on mechanical properties of a porous polymethylmethacrylate space maintenance device. *J Med Device* 9: 024501.
37. Wang L, et al. (2013) Characterization of porous polymethylmethacrylate space maintainers for craniofacial reconstruction. *J Biomed Mater Res B Appl Biomater* 101: 813–825.
38. Gibson-Corley KN, Olivier AK, Meyerholz DK (2013) Principles for valid histopathologic scoring in research. *Vet Pathol* 50:1007–1015.
39. Vaux DL, Fidler F, Cumming G (2012) Replicates and repeats–What is the difference and is it significant? A brief discussion of statistics and experimental design. *EMBO Rep* 13:291–296.
40. Yan YB, et al. (2014) A pilot trial on the molecular pathophysiology of traumatic temporomandibular joint bony ankylosis in a sheep model. Part II: The differential gene expression among fibrous ankylosis, bony ankylosis and condylar fracture. *J Craniomaxillofac Surg* 42:e23–e28.
41. Redmer DA, Aitken RP, Milne JS, Reynolds LP, Wallace JM (2005) Influence of maternal nutrition on messenger RNA expression of placental angiogenic factors and their receptors at midgestation in adolescent sheep. *Biol Reprod* 72:1004–1009.
42. Dorotka R, et al. (2005) Repair of articular cartilage defects treated by microfracture and a three-dimensional collagen matrix. *Biomaterials* 26:3617–3629.